

Alma Mater Studiorum Università di Bologna
Archivio istituzionale della ricerca

DNA Damage Detection by 53BP1: Relationship to Species Longevity

This is the final peer-reviewed author's accepted manuscript (postprint) of the following publication:

Published Version:

Croco, E., Marchionni, S., Bocchini, M., Angeloni, C., Stamato, T., Stefanelli, C., et al. (2017). DNA Damage Detection by 53BP1: Relationship to Species Longevity. JOURNALS OF GERONTOLOGY SERIES A-BIOLOGICAL SCIENCES AND MEDICAL SCIENCES, 72(6), 763-770 [10.1093/gerona/glw170].

Availability:

This version is available at: <https://hdl.handle.net/11585/600660> since: 2017-07-20

Published:

DOI: <http://doi.org/10.1093/gerona/glw170>

Terms of use:

Some rights reserved. The terms and conditions for the reuse of this version of the manuscript are specified in the publishing policy. For all terms of use and more information see the publisher's website.

This item was downloaded from IRIS Università di Bologna (<https://cris.unibo.it/>).
When citing, please refer to the published version.

(Article begins on next page)

This is the final peer-reviewed accepted manuscript of:

Croco, E.; Marchionni, S.; Bocchini, M.; Angeloni, C.; Stamato, T.; Stefanelli, C.; Hrelia, S.; Sell, C.; Lorenzini, A. DNA Damage Detection by 53BP1: Relationship to Species Longevity. *The Journals of Gerontology: Series A* **2017**, 72 (6), 763–770.

The final published version is available online at:

<https://doi.org/10.1093/gerona/glw170>.

Rights / License:

The terms and conditions for the reuse of this version of the manuscript are specified in the publishing policy. For all terms of use and more information see the publisher's website.

This item was downloaded from IRIS Università di Bologna (<https://cris.unibo.it/>)

When citing, please refer to the published version.

DNA damage detection by 53BP1: relationship to species longevity

Croco E.¹, Bocchini M.², Marchionni S.², Angeloni C.¹, Stamato T.³, Stefanelli C.¹, Hrelia S.¹, Sell C.⁴, Lorenzini A.^{2*}

¹ Department of Life Quality Studies, University of Bologna, Italy

² Department of Biomedical and Neuromotor Sciences, University of Bologna, Italy

³ The Lankenau Institute for Medical Research, Wynnewood, PA, USA

⁴ Department of Pathology, Drexel University College of Medicine, Philadelphia, PA, USA

* To whom correspondence should be addressed:

Antonello Lorenzini, PhD

Department of Biomedical and Neuromotor Sciences

University of Bologna

Via Irnerio 48, 40126 Bologna, Italy

Tel: +39 051 2091208;

Fax: +39 051 2091208;

Email: antonello.lorenzini@unibo.it

ABSTRACT

In order to examine potential differences in genomic stability, we have challenged primary fibroblasts from five different mammalian species of variable longevity with the genotoxic agents, etoposide and neocarzinostatin. We report that cells from longer-lived species exhibit more tumor protein p53 binding protein 1 (53BP1) foci for a given degree of DNA damage relative to shorter-lived species. The presence of a greater number of 53BP1 foci was associated with decreased DNA fragmentation and a lower percentage of cells exhibiting micronuclei. These data suggest that cells from longer-lived species have an enhanced DNA damage response. We propose that the number of 53BP1 foci that form in response to damage in primary cells can reflect the intrinsic capacity of the cell to detect and respond to DNA damage.

KEY WORDS

53BP1, longevity, genomic stability, DNA damage foci, micronuclei

INTRODUCTION

Double-strand breaks (DSBs) are the most harmful DNA lesions a cell can encounter. In mammals, non-homologous end-joining (NHEJ) is the cellular mechanism responsible for repairing the majority of DSBs (1). This is due to the fact that NHEJ is active throughout the cell cycle, whereas homologous recombination (HR) is typically active only during the S and G₂ phases (2). Moreover, the majority of cells in the adult body are in G₀. At the sites of DSBs, nuclear foci of phosphorylated histone H2AX (γ H2AX) and tumor protein p53 binding protein 1 (53BP1) can be detected by immunofluorescence and are widely used as DNA damage markers since their abundance has been reported to correlate very closely with the degree of genotoxic insult (reviewed in Rothkamm et al., 2015). 53BP1 accumulates in DNA damage foci after the occurrence of DSBs in order to facilitate NHEJ repair (4). Previous work has shown that 53BP1 is involved in activation of the DNA damage response during the G₁, S, and G₂ phases of the cell cycle (5)(6)(7).

We have previously observed an unexpected difference in the formation of DNA damage foci between human and mouse cells following exposure to the same concentration of neocarzinostatin (NCS). Despite similar exposure to the DNA-damaging agent, human cells exhibited a significantly greater number of 53BP1 foci compared with mouse cells. The greater abundance of foci in human cells correlated inversely with the appearance of micronuclei, which represent the presence of severe genomic damage (8). We have also reported an impressive correlation between mammalian longevity and the capacity of nuclear proteins to bind DNA ends, which appears to be largely dependent on increased expression of the evolutionarily highly conserved heterodimer Ku80/Ku70 (9). The DNA end-binding assay represents, the accumulation of proteins required for the initial DNA damage recognition, a necessary step before a cell can proceed with repair, cell cycle arrest or apoptosis. These data persuaded us to conduct a deeper investigation into the relationship between the appearance of markers of DNA damage and mammalian longevity.

To this end, we have compared fibroblast cells from mouse (maximum longevity, 4 y; weight, 20.5 g), cow (maximum longevity, 20 y; weight, 750 Kg), dog (maximum longevity, 24 y; weight, 40.0 Kg), little brown bat (maximum longevity, 34 y; weight, 10.0 g), and human (maximum longevity, 122 y; weight, 62.0 Kg) in their response to the genotoxic insult caused by etoposide (ETO) and NCS. ETO is a poison that binds reversibly to

topoisomerase II α/β to block re-ligation of cleaved DNA strands, causing DSBs (10), while NCS is a macromolecular chromoprotein antibiotic that causes single- and double-strand breaks (11). Our experimental approach was based on the assumption that the biological mechanisms that facilitate longevity are cell autonomous and thus will be reflected in fundamental cellular processes. Consequently, these mechanisms can be studied in cell culture away from the complexity of the whole organism. With the present work, we propose that quantitative, species-specific differences in 53BP1 foci formation observed following exposure to genotoxic agents correlate with differences in lifespan and adult body mass, suggesting a new interpretation of nuclear foci as markers of a species' ability to detect and mitigate DNA damage to ensure maximal longevity.

MATERIAL AND METHODS

Cell culture

All fibroblast strains and lines used are described in Supplemental Table 1. Fibroblast strains from mouse, little brown bat, dog, and cow were established as previously described (12). Adult human fibroblasts were obtained from Claudio Franceschi (DIMES, University of Bologna).

Cells were maintained in Minimum Essential Medium (MEM) with Earle's Salts and L-glutamine containing 10% fetal bovine serum (FBS), MEM vitamins and amino acids, and penicillin-streptomycin (all from Sigma Aldrich, St. Louis, Mo). Fibroblasts were passaged weekly and cumulative population doubling (PD) was determined as previously described (13). With the exception of the immortalized 3T3 mouse line and little brown bat strains that had undergone spontaneous immortalization, lines displayed cellular senescence and were used for all experiments at approximately half way through their replicative lifespan.

Genotoxic treatment

Cells were treated with ETO and NCS (both from Sigma Aldrich, St. Louis, Mo). S phase was chosen as the most appropriate time for exposure to genotoxic stress because a previous study determined that differences in susceptibility to genotoxic damage between human and mouse cells were most apparent in S-G₂ (8). Additionally, topoisomerase II inhibitors are most effective during DNA replication in S phase (14). Cultures were initially arrested in G₀ by serum starvation for 48 hours (h) in serum-free medium. Cells were then stimulated to enter the cell cycle by the addition of fresh complete medium with 10% FBS. For each species, the time following FBS stimulation required for entry into S phase was defined by cell cycle analysis (data not shown). Mouse and bat cells were stimulated in complete medium with 10% FBS for 16 h; dog, cow, and human for 18 h. Once synchronized, cells were treated in complete serum-free medium to avoid the potential for interference of serum on drug bioavailability. Low-dose (LD) and high-dose (HD) concentrations of the genotoxic agents ETO (LD-ETO 5 μ M and HD-ETO 50 μ M) and NCS (LD-NCS 2.25 μ M and HD-NCS 22.5 μ M) were used, respectively. Low

doses were used for the foci formation and micronuclei assays, and Western blotting. High doses were used for the comet assay. Both doses were used for the methylthiazoletetrazolium (MTT) assay.

Immunofluorescence determination of 53BP1 and γ H2AX foci

Fibroblasts were seeded onto glass coverslips, synchronized as previously described, and treated with LD-ETO or LD-NCS for 6 or 2 h, respectively. Cells were fixed immediately after treatment or at indicated times after damage in 4% paraformaldehyde for 10 minutes and permeabilized in 0.2% Triton X-100 in PBS for 5 minutes. Cells were washed once in PBS and blocked for 30 minutes in 4% BSA in PBS containing Tween-20 (PBST), after which they were incubated with anti-53BP1 (NB 100-304 or NB 100-305, Novus Biologicals, Littleton, Co) and anti- γ H2AX (05-636, clone JBW301, Merck Millipore, Darmstadt, Germany) in 1% BSA-PBST buffer for 2 h at 37°C in a humidified chamber. Anti-53BP1 antibody (NB 100-304) binds, in tested species, epitopes with homologies that range between 90% and 92% compared to the human epitope. Anti- γ H2AX antibody, used for human and mouse, binds an epitope with a homology of 90% between these two species. Slides were washed three times in PBST and incubated with AlexaFluor555-conjugated goat anti-rabbit and AlexaFluor488-conjugated goat anti-mouse secondary antibody (respectively #4413S and #4408S, Cell Signaling, Danvers, Ma) in 1% BSA-PBST for 1 h. Cells were washed three times, stained with DAPI, and mounted with Vectashield mounting medium (Vector Laboratories, Burlingame, Ca) before visualizing. Images were captured using an Olympus BX61 fluorescence microscope (Tokyo, Japan) equipped with a Hamamatsu ORCA-ER camera (Hamamatsu City, Japan) or an Olympus IX50 equipped with a Diagnostic Instruments 9.0 Monochrome - 6 camera (Sterling Heights, Mi). Clearly identifiable 53BP1 or γ H2AX foci inside the nucleus were counted as positive foci. Nuclei were scored as containing: 53BP1 foci (F) < 5 ; $5 \leq F < 20$; $F \geq 20$. Nuclei with fewer than 5 foci were considered foci-negative because this number of foci was common in untreated cells.

Micronuclei assay

Cells synchronized in S phase as previously described were treated with LD-ETO or LD-NCS for 6 or 2 h, respectively. At the indicated times (see Figures), cells were fixed in 4% paraformaldehyde for 10 minutes and permeabilized in 0.2% Triton X-100 in PBS for 1 minute. Fixed cells were stained with DAPI and washed with PBS. Cells were mounted with Vectashield and scored using fluorescence microscopy as above. Micronuclei, defined as DAPI-positive bodies that were morphologically identical but smaller than the nucleus, were scored according to Thomas and Fenech (15). Cells were considered micronucleus-positive if they contained, at least, one micronucleus.

DNA synthesis assessment

Fibroblasts were seeded onto glass coverslips, synchronized as described above, and treated with LD-ETO for 6 h. 10 μ M BrdU pulse, with different lapse of time (see Figures), was performed to assess DNA synthesis. Cells were fixed at the desired time point, as previously described, and were treated with 1M HCl for 45 minutes at room temperature. HCl was then neutralized with borate buffer and cells were washed once in PBS and blocked for 30 minutes in 4% BSA in PBST. Cells were incubated with an anti-BrdU antibody (clone BU20A, eBioscience, San Diego, Ca) in 1% BSA-PBST buffer for 2 h at 37°C in a humidified chamber. Slides were then washed three times in PBST and incubated in AlexaFluor488-conjugated goat anti-mouse secondary antibody in 1% BSA-PBST for 1 h to label BrdU incorporation.

Comet assay

The microgel electrophoretic technique was performed utilizing the neutral lysis method which detects DSBs (16). From a population of synchronized cells, a single-cell suspension was prepared by trypsin disaggregation. Disaggregated cells were counted and treated with HD-ETO and HD-NCS for 30 minutes at room temperature and were then re-suspended in 1% low-melting agarose. The low-melting cellular suspension was seeded onto slides and cells were lysed by placing the slides in a humid chamber at 37°C with 2% SDS, 0.05M EDTA, 0.5 mg/ml proteinase K for at least 18 h. Lysis was performed under neutral conditions to detect DSBs. After lysis,

slides were washed two times in 0.5X TBE buffer. Electrophoresis was carried out at 30 v/cm for 15 minutes in 0.5X TBE buffer. For visualization of DNA damage, slides were stained with DAPI and observed using fluorescence microscopy as described above. Cells with DNA damage appeared as comets. One hundred comets were scored for each species and each time point, and analyzed with Open Comet (17) image analysis software. Individual comet images were scored for several features including tail length and percentage DNA in tail.

Cellular viability assay

Fibroblast viability was evaluated in terms of mitochondrial activity, by conversion of the dye MTT to insoluble formazan (18). Cells were seeded in 96-well plates and treated with low and high doses of ETO and NCS for 6 and 2 h, respectively. At the indicated times (see Figures), cells were washed with PBS and incubated in MTT (5 mg/mL) in PBS for 2 h. After removal of MTT, formazan crystals were dissolved with DMSO (all from Sigma Aldrich, St. Louis, Mo) and the amount of formazan was measured at $\lambda = 570$ nm (ref. $\lambda = 690$ nm) with a spectrophotometer (Victor² Multilabel Counter, PerkinElmer, Waltham, Ma). All experiments were repeated at least two times, with each comprising an evaluation of five wells per treatment. Mitochondrial activity in treated cells was calculated as a percentage relative to control cells according to the formula: (absorbance of treated fibroblasts/absorbance of untreated fibroblasts) \times 100.

Statistical analysis

All statistical analyses were performed using Graphpad Software Inc (La Jolla, Ca). Maximum human longevity is 122 years. In the figures captions and in the correlation analysis it is adjusted to 90 years to account for the fact that, for the others species, only small cohorts were used to determine maximum longevity, and 90 years seems a more realistic estimate for a random sample of humans.

RESULTS

53BP1 foci formation after damage

Cells were exposed to either LD-ETO or LD-NCS during S phase and were monitored at specific time intervals, up to three days after damage. **Figure 1.A** presents data from cells treated with LD-ETO. Time-course analysis after LD-ETO treatment revealed a peak in 53BP1 foci formation between 2 and 10 h in all species (**Figure 1.C**), followed by a gradual decline in the percentage of foci-positive nuclei. Interestingly, longer-lived species showed a higher percentage of nuclei with 53BP1 foci. Human cells, derived from the longest-lived species, exhibited the highest percentage of foci when compared to all other species, with statistical significance observed consistently at 2 and 24 h post damage. Moreover, human cells seemed to retain a higher number of foci over time. Because we previously observed that 24 h was required for visible foci to form in cells treated with 1.5 µg/mL of NCS (8), we scored foci from 24 to 72 h after damage with this agent. Similar to results with LD-ETO, longer-lived species exhibited a higher percentage of cells with more than five foci per nucleus in response to LD-NCS. Human cells showed the highest percentage of cells with more than five 53BP1 foci (**Figure 1.B**). To monitor cell survival under these conditions, we also measured metabolic activity as the capacity to convert MTT to formazan (**Figure 2**). LD treatments did not cause a significant reduction in MTT activity, whereas HD treatments did.

Co-localization of 53BP1 with γ H2AX

Since DSBs can be repaired by either NHEJ or HR, we conducted experiments aimed at evaluating which repair pathway was more likely activated in the nuclear regions marked by 53BP1. **Figure 3.A** shows that with genotoxic treatment, 53BP1 foci co-localize with γ H2AX foci in the vast majority of cases in both mouse and human cells. Between 1, 2 and 10 h after treatment, every hundred 53BP1 foci, more than eighty co-localized with γ H2AX in both species (**Figure 3.B**). Because co-localization of 53BP1 and γ H2AX in foci is usually interpreted as a marker of NHEJ (19)(20)(21), these data suggest that this repair pathway is favored in both species under our experimental conditions.

DNA damage induces cell cycle arrest

Progression through the cell cycle was monitored by cytofluorimetric measurement of DNA content in mouse, dog, cow, and human cells. Cyclin A and Nek 4 expression was examined in species for which antibodies with conserved epitopes were available. These species included mouse, cow, little brown bat, and human (**Supplementary Figures 1 and 2**). Cytofluorimetric analysis revealed a significant shift in the cell cycle profile in all four species tested. In treated cells, there was an increased percentage of cells in the S and G₂ phases of the cell cycle; Especially G₂ in mouse and S in dog, cow, and human. Increased expression in cyclin A in all treated cells confirmed a larger proportion of cells in G₂ arrest. This was evident in all species, but especially pronounced in human and cow. In addition, the expression of Nek 4, a recently described regulator of both DNA-PK association with DNA damage and entry into senescence (22), also increased following damage.

To better observe differences in the efficiency of cell cycle arrest following damage, we exposed mouse and human cells to LD-ETO and pulsed them with BrdU. Cells were analyzed for the percentage of cells synthesizing DNA (BrdU-positive nuclei) and the percentage that harbor BrdU-positive 53BP1 foci (BrdU staining only in damage foci) at time points from 14 to 72 h after damage. At 14 h, human cell populations contained a lower percentage of cells synthesizing DNA compared with mouse cells, but a similar percentage of cells with BrdU foci. At 24 h, the percentage of cells incorporating BrdU increased for both species, indicating progression through the cell cycle. Again, the human population had a lower percentage of cells incorporating BrdU, but a higher percentage of BrdU in foci, suggesting a more active repair (**Supplemental Figure 3**).

DNA fragility across species

We next evaluated DNA fragility after genotoxic stress. We performed comet assays under neutral conditions for the detection of DNA damage at the level of the individual cell. Comet tails obtained with the LD-ETO and LD-NCS used in long-term experiments were too short to measure significant differences. For this reason, higher doses (HD) of ETO and NCS were used for comet assays. **Figure 4** contains data from cells treated with HD-

10

ETO and HD-NCS for 60 and 30 minutes, respectively. Genotoxic treatments resulted in DNA fragmentation and the appearance of comet tails. We calculated fold increase in the percentage of DNA in comet tails and in tail moments (measures obtained by multiplying tail length by percentage DNA in tail). After both HD treatments, we observed a significant increase in the percentage of tail DNA in all species. Although the results of the two measure of DNA damage (percent tail DNA and tail moment) did not overlap, cells from the mouse, the shortest-lived species in the panel, had significantly greater DNA fragmentation in all instances. The longest-lived species (human) and the largest (cow) exhibited the least amount of damage in the comet assay. Since DNA damage repair is activated within minutes of damage (23), we expect that fast repair mechanisms rather than chromatin structural strength are responsible for the observed differences among species.

Measuring unresolved damage

To assess the amount of unresolved damage in each species after genotoxic stress, we scored micronuclei formation 0, 24, 48 and 72 h after damage. Micronuclei originate from chromosome fragments or whole chromosomes that lag behind at anaphase (15). We observed that shorter-lived species have a higher percentage of nuclei with ≥ 1 micronucleus. In particular, mouse, the shortest-lived species, showed the highest percentage of micronuclei at all time points both after LD-ETO and LD-NCS treatments (**Figure 5a and 5b, respectively**). As a demonstration that micronuclei arise only in cycling cells, we also scored them in BrdU-positive cells (**Figure 5c**). The steady state level of the 53BP1 protein was also assessed following genotoxic stress. Independently from treatment time, whole lysates show a multiband pattern of 53BP1, suggesting the existence of different modifications of the protein (**Supplementary Figure 4a**). Densitometric analysis of multiple experiments including all four visible bands is shown in **Supplementary Figure 4b**. It appears that protein levels do not change substantially during the 24 h following LD-ETO treatment (except for the 24 h time point in dog cells). This suggests that 53BP1 is a constitutive protein. Mouse and dog cells have significantly lower level compared with human cells. More generally, the larger and/or longer-lived species (cow, bat and human) appear to possess higher 53BP1 protein amounts although these differences are always below one fold.

53BP1 foci are inversely correlated with micronuclei abundance

To interpret the relationship between 53BP1 foci, micronuclei, and lifespan, we plotted the data for 53BP1 foci formation and micronuclei, with species longevity. We used data from the 72 h time point following exposure to NCS, since this treatment produces the highest number of long-lasting foci interpretable as DNA Segments of Chromatin Reinforcing Senescence (abbreviated in SCARS) as suggested by Rodier and colleagues (24). Micronuclei were inversely related to long-lasting foci ($R^2=0.86$; $p=0.021$) (**Figure 6.A**). Additionally, while long-lasting foci were strongly and positively related with longevity ($R^2=0.87$; $p=0.020$; **Figure 6.B**), micronuclei were negatively related ($R^2=0.59$), although this relationship did not reach significance in this data set. (**Figure 6.D**). Like maximum longevity, body mass was also positively related with long-lasting foci ($R^2=0.36$; **Figure 6.C**) and negatively related with micronuclei ($R^2=0.35$; **Figure 6.E**), although neither association reached significance in this data set. These data suggest that both longevity and body mass are related to genome surveillance and stability, but that longevity is more strongly related than body mass.

DISCUSSION

The aim of the present work is to understand the biological significance of the appearance of a higher number of DNA damage induced 53BP1 foci in human cells compared to mouse cells (8). This initial finding was counterintuitive since a higher number of foci is generally interpreted as evidence of a greater amount of damage. However, using direct measurements of DNA damage such as the comet assay (**Figure 4**) and micronuclei counts (**Figure 5**), we report here that longevity and, to a lesser extent, adult body size are indeed associated with higher genomic stability. To explain this apparent contradiction between the direct measurement of DNA damage and 53BP1 foci count we propose the following model graphically described in **Figure 7**:

In mammals, DNA and associated proteins (histones) are chemically equivalent and similarly fragile when exposed to the same genotoxic damage. In a single species, 53BP1 foci abundance is proportional to the

amount of damage. However, the difference observed in foci abundance between species is not due to different levels of damage but to different capacities to detect this damage. We suggest the possibility that foci represent a primary DNA damage response. Thus, within each species, a larger amount of damage correlates with an increase in the number of foci. However, when between-species comparisons are made, longer-lived or larger species produce more foci for a similar amount of DNA damage because are more efficient in this primary DNA damage response. A potential downstream consequence of this difference is that long-lived or larger species may be more prone to activate cell cycle arrest and DNA repair, apoptosis, or senescence. The choice between these options will likely depend on the interactions between the level of damage and other cellular and extracellular conditions.

The presence of 53BP1 foci was studied in a large investigation of skin-derived fibroblasts from 100 human donors aged 20 to 90 years. It was observed a positive correlation between donor age and 53BP1 foci and also a positive correlation between 53BP1 foci and micronuclei in support of the concept that, inside a single species, 53BP1 represents a marker of the endured DNA damage (25).

In support of our model, we find that species with significant longevity (human and little brown bat) and species with a combination of moderate longevity and large adult body size (cow) demonstrate a higher level of early repair as measured by the comet assay. Additionally, mouse, the species in our study in which short life span associates with small body mass, shows a significantly higher level of micronuclei compared with all other longer-lived or larger species. Concerning 53BP1 foci abundance: mouse cells, and to a lesser extent cow cells, produce fewer foci after damage compared with the other species. Little brown bat and human, the two species with the longest life span, show the highest level of foci both at shorter time points (see LD-ETO treatment) and at longer time points (see LD-NCS treatment).

Rodier and colleagues have suggested to consider persistent foci (ie, foci that have not resolved in 24 h) as DNA SCARS (24). Our data support this proposal. DNA-damage—induced cellular senescence could be an effective way to guarantee genomic stability when multiple cellular divisions are required to attain a large body size or to guarantee tissue turnover during a long lifespan.

Although our investigation includes a small number of species, we have chosen a set of species with a wide range in maximum longevity and adult body mass in an attempt to dissociate the potential effects of these two parameters on genome stability. Species longevity and body mass are known to correlate with each other (26) and it is reasonable to expect that they both correlate positively with genome stability. The common mammalian ancestor was small sized and probably short lived [(27) and references therein]. It is reasonable to suggest that a variety of mechanisms have evolved to ensure the genomic stability required for larger body size and longer life span. Some of these mechanisms will be important especially for long-lived species while other will be important especially for species with large bodies, moreover some will be common to several (or perhaps all) species, while other will be unique to particular orders, families or species. We believe, interpreting the present work in the context of our previous observation on DNA end binding (9), that improving DNA damage detection could be an evolutionary conserved mechanism to provide the increased genomic stability required in long-lived and large species to prevent respectively early life tissue dysfunctions and tumors development. The relevance of this observation goes beyond the aging field since scientists studying DNA repair pathways commonly use cells lines derived from multiple species. Additionally, DNA damage foci are already studied at the clinical level as potential markers for radiosensitivity of tumors (28) and of patients' normal tissues (29). Clinicians, therefore, will have to interpret correctly data obtained by researcher using species other than human to design the most adapt therapy for our species.

ACKNOWLEDGEMENT

We thank Leslie Sell, PhD for editorial assistance.

FUNDING

This work was supported by RFO 2014 of University of Bologna to AL. Grant AG39799 to CS from the National Institutes of Health/National Institute on Aging.

REFERENCES

1. Kakarougkas,A. and Jeggo,P.A. (2014) DNA DSB repair pathway choice: an orchestrated handover mechanism. *Br. J. Radiol.*, **87**, 20130685.
2. Rothkamm,K., Krüger,I., Thompson,L.H. and Löbrich,M. (2003) Pathways of DNA double-strand break repair during the mammalian cell cycle. *Mol. Cell. Biol.*, **23**, 5706–15.
3. Rothkamm,K., Barnard,S., Moquet,J., Ellender,M., Rana,Z. and Burdak-Rothkamm,S. (2015) DNA damage foci: Meaning and significance. *Environ. Mol. Mutagen.*, **56**, 491–504.
4. Dimitrova,N., Chen,Y.-C.M., Spector,D.L. and de Lange,T. (2008) 53BP1 promotes non-homologous end joining of telomeres by increasing chromatin mobility. *Nature*, **456**, 524–528.
5. Wang,B., Matsuoka,S., Carpenter,P.B. and Elledge,S.J. (2002) 53BP1, a mediator of the DNA damage checkpoint. *Science*, **298**, 1435–8.
6. Cescutti,R., Negrini,S., Kohzaki,M. and Halazonetis,T.D. (2010) TopBP1 functions with 53BP1 in the G1 DNA damage checkpoint. *EMBO J.*, **29**, 3723–32.
7. Fernandez-Capetillo,O., Chen,H., Celeste,A., Ward,I., Romanienko,P.J., Morales,J.C., Naka,K., Xia,Z., Camerini-otero,R.D., Motoyama,N., *et al.* (2002) DNA damage-induced G 2 – M checkpoint activation by histone H2AX and 53BP1. **4**, 993–998.

8. Fink,L.S., Roell,M., Caiazza,E., Lerner,C., Stamato,T., Hrelia,S., Lorenzini,A. and Sell,C. (2011) 53BP1 contributes to a robust genomic stability in human fibroblasts. *Aging (Albany. NY).*, **3**, 836–845.
9. Lorenzini,A., Johnson,F.B., Oliver,A., Tresini,M., Smith,J.S., Hdeib,M., Sell,C., Cristofalo,V.J. and Stamato,T.D. (2009) Significant correlation of species longevity with DNA double strand break recognition but not with telomere length. *Mech. Ageing Dev.*, **130**, 784–792.
10. Soubeyrand,S., Pope,L. and Haché,R.J.G. (2010) Topoisomerase IIalpha-dependent induction of a persistent DNA damage response in response to transient etoposide exposure. *Mol. Oncol.*, **4**, 38–51.
11. Goldberg,I.H. (1987) Free radical mechanisms in neocarzinostatin-induced DNA damage. *Free Radic. Biol. Med.*, **3**, 41–54.
12. Lorenzini,A., Tresini,M., Austad,S.N. and Cristofalo,V.J. (2005) Cellular replicative capacity correlates primarily with species body mass not longevity. *Mech. Ageing Dev.*, **126**, 1130–1133.
13. Gibson,G.E., Tofel-Grehl,B., Scheffold,K., Cristofalo,V.J. and Blass,J.P. (1998) A reproducible procedure for primary culture and subsequent maintenance of multiple lines of human skin fibroblasts. *Age (Omaha).*, **21**, 7–14.
14. Gorczyca,W., Gong,J., Ardelt,B., Traganos,F. and Darzynkiewicz,Z. (1993) The cell cycle related differences in susceptibility of HL-60 cells to apoptosis induced by various antitumor agents. *Cancer Res.*, **53**, 3186–92.
15. Thomas,P. and Fenech,M. (2011) Cytokinesis-block micronucleus cytome assay in lymphocytes. *Methods Mol. Biol.*, **682**, 217–34.
16. Olive,P.L. and Banáth,J.P. (2006) The comet assay: a method to measure DNA damage in individual cells. *Nat. Protoc.*, **1**, 23–9.
17. Gyori,B.M., Venkatachalam,G., Thiagarajan,P.S., Hsu,D. and Clement,M.-V. (2014) OpenComet: an automated tool for comet assay image analysis. *Redox Biol.*, **2**, 457–65.

18. Mosmann,T. (1983) Rapid colorimetric assay for cellular growth and survival: application to proliferation and cytotoxicity assays. *J. Immunol. Methods*, **65**, 55–63.
19. Orsburn,B., Escudero,B., Prakash,M., Gesheva,S., Liu,G., Huso,D.L. and Franco,S. (2010) Differential requirement for H2AX and 53BP1 in organismal development and genome maintenance in the absence of poly(ADP)ribosyl polymerase 1. *Mol. Cell. Biol.*, **30**, 2341–52.
20. Lu,J. and Matunis,M.J. (2013) A mediator methylation mystery: JMJD1C demethylates MDC1 to regulate DNA repair. *Nat. Struct. Mol. Biol.*, **20**, 1346–8.
21. Nikolova,T., Dvorak,M., Jung,F., Adam,I., Krämer,E., Gerhold-Ay,A. and Kaina,B. (2014) The γ H2AX assay for genotoxic and nongenotoxic agents: comparison of H2AX phosphorylation with cell death response. *Toxicol. Sci.*, **140**, 103–17.
22. Nguyen,C.L., Possemato,R., Bauerlein,E.L., Xie,A., Scully,R. and Hahn,W.C. (2012) Nek4 regulates entry into replicative senescence and the response to DNA damage in human fibroblasts. *Mol. Cell. Biol.*, **32**, 3963–77.
23. Mari,P.-O., Florea,B.I., Persengiev,S.P., Verkaik,N.S., Brüggerwirth,H.T., Modesti,M., Giglia-Mari,G., Bezstarosti,K., Demmers,J.A.A., Luijckx,T.M., *et al.* (2006) Dynamic assembly of end-joining complexes requires interaction between Ku70/80 and XRCC4. *Proc. Natl. Acad. Sci. U. S. A.*, **103**, 18597–602.
24. Rodier,F., Muñoz,D.P., Teachenor,R., Chu,V., Le,O., Bhaumik,D., Coppé,J.-P., Campeau,E., Beauséjour,C.M., Kim,S.-H., *et al.* (2011) DNA-SCARS: distinct nuclear structures that sustain damage-induced senescence growth arrest and inflammatory cytokine secretion. *J. Cell Sci.*, **124**, 68–81.
25. Waaijer,M.E.C., Croco,E., Westendorp,R.G.J., Slagboom,P.E., Sedivy,J.M., Lorenzini,A. and Maier,A.B. (2016) DNA damage markers in dermal fibroblasts in vitro reflect chronological donor age. *Aging (Albany. NY)*, **8**, 147–57.
26. Austad,S.N. (2005) Diverse aging rates in metazoans: Targets for functional genomics. *Mech. Ageing Dev.*, **126**, 43–49.

27. O'Leary,M.A., Bloch,J.I., Flynn,J.J., Gaudin,T.J., Giallombardo,A., Giannini,N.P., Goldberg,S.L., Kraatz,B.P., Luo,Z.-X., Meng,J., *et al.* (2013) The placental mammal ancestor and the post-K-Pg radiation of placentals. *Science*, **339**, 662–7.
28. Willers,H., Gheorghiu,L., Liu,Q., Efstathiou,J.A., Wirth,L.J., Krause,M. and von Neubeck,C. (2015) DNA Damage Response Assessments in Human Tumor Samples Provide Functional Biomarkers of Radiosensitivity. *Semin. Radiat. Oncol.*, **25**, 237–50.
29. Bourcier,C., Lacombe,J., Solassol,J., Mange,A., Pèlegri,A., Ozsahin,M. and Azria,D. (2015) Late side-effects after curative intent radiotherapy: Identification of hypersensitive patients for personalized strategy. *Crit. Rev. Oncol. Hematol.*, **93**, 312–9.

TABLE AND FIGURES LEGENDS

Figure 1. Long-lived species exhibit the highest percentage of 53BP1 foci. During S phase, cells were exposed to either LD-ETO (5 μ M) for 6 h or LD-NCS (2.25 μ M) for 2 h in serum free medium. After treatment, cells were washed and fed with regular growth medium (10% FBS). The respective maximum longevity of each species is reported in parenthesis in years (y). **A)** LD-ETO treated cells were fixed either during and right after treatment at the following time points: 2, 6, 10, 24, 48, or 72 h following damage and stained for 53BP1 antibody. **B)** NCS treated cells were fixed at 24, 48 and 72 h. Untreated fibroblasts were included as controls. From 200 to 400 cells per time point were counted and means \pm s.e.m. were calculated from two to six experiments. Cells scored for 53BP1 foci (F) were grouped into: $F < 5$, $5 \leq F < 20$ foci and $F > 20$ foci per nucleus. The histogram bars show the percent of nuclei with 53BP1 foci > 5 (obtained summing $5 \leq F < 20$ and $F > 20$). Statistical significance is referred to the comparison of all the species to the equivalent time point in human. Statistical analysis: Anova test followed by Tukey's Multiple Comparison Test ($P < 0.05$). **C)** Time course curve shows the trend of foci formation after LD-ETO treatment, in all species, from 0 to 72 h. **D)** Foci formation induced by LD-ETO evaluated by immunofluorescence staining, at 24 h after treatment beginning.

Figure 2. Low dose treatments induce a low cytotoxic effect in all species. Fibroblast viability was evaluated with the colorimetric MTT assay in untreated (CTRL) and treated cells (LD and HD of ETO and NCS) at 24, 48 and 72 h. Statistical analysis: Anova test followed by Tukey's Multiple Comparison Test ($P < 0.05$). Anova test has been performed comparing treated sample to control cells at the relative time point. \bullet = p value < 0.05 ; \circ = p value > 0.05 .

Figure 3. 53BP1 co-localize with γ H2AX after LD-ETO treatment. **A)** Representative immunofluorescence images of human and mouse nuclei stained with the indicated antibodies following LD-ETO treatment. Right

images show merged signals. **B)** 53BP1 co-localization with γ H2AX in nuclear foci 1, 2 and 10 h after LD-ETO treatment. Statistical analysis: T-Student test followed by paired test (p value = NS).

Figure 4. Human DNA generally appears more or equally resistant to fragmentation when compared to other species. Quantification of percent DNA in comets tails (A-B) and quantification of Tail moment (C-D) after HD-ETO (for 60 minutes) and HD-NCS (for 30 minutes) are presented in a box plot showing means \pm s.e.m and whiskers representing 10-90 percentile. For both treatments, data were obtained from two independent experiments. Lifespan in years and body mass in Kg of species (E-F). Statistical analysis: Kruskal-Wallis analysis. The data from a single species was compared to each individual species. Significant difference (p value <0.0001) between pairs of species is indicated by the presence of the initials above the box plot for each species (M = mouse; D = dog; C = cow; B = bat; H = human). G) Representative comets of untreated (CTRL) and HD-ETO treated fibroblasts.

Figure 5. Short-lived species have higher percentage of Micronuclei (MN). All cells were synchronized in G_0 phase by 48 h incubation in serum free medium. Cells were then stimulated to enter into the S-phase by adding complete growth medium (10% FBS) as described in materials and methods. Cells in S-phase were treated in serum free medium with LD-ETO (**A**), LD-NCS (**B**) or LD-ETO with a BrdU pulse (**C**, Cells were pulsed with BrdU for all the length of the treatment); cells were washed and fed with growth medium and allowed to recover from damage. Micronuclei were scored at 24, 48 and 72 h after the beginning of the treatment. Means \pm s.e.m of the percentage of nuclei with MN >1 , scored on a minimum of 400 cells are presented. Means were calculated from two to six experiments. In all instances, control cells (CTRL) are cells at 24 h past complete growth medium addition. The respective maximum longevity of each species is reported in parenthesis in years (a). Statistical analysis: Anova test followed by Tukey's Multiple Comparison Test (p <0.0001). Statistical significance was tested through comparison of each species to the equivalent time point in mouse.

Figure 6. Correlation of 53BP1 foci and MN with maximum longevity and adult body mass. Correlations were examined using data collected at 72 h after NCS treatment for both 53BP1 Foci and MN. Panel **A** contains the inverse correlation between 53BP1 foci and MN. Panels (B) and (C) contain positive correlations between 53BP1 foci and longevity and body mass respectively. Panels (D) and (E) contain the positive correlation between MN and longevity and body mass respectively. All values were natural logarithm transformed. Coefficient of determinations and p values are shown.

Figure 7. Proposed model. Red dots represent 53BP1 foci while lightning images represent DNA damage. See discussion for model explanation.

SUPPLEMENTARY MATERIAL AND METHODS

SDS-PAGE and Western blotting

For SDS-PAGE, 50 micrograms of cell extracts in RIPA buffer (50mM Tris, 150mM NaCl, 1% NP-40, 0.1% SDS, 0.5% sodium deoxycholate, 1mM PMSF, 1 µg/mL leupeptin, 1 µg/mL pepstatin) were loaded onto polyacrylamide gels. Gels were transferred to nitrocellulose membranes and blocked for 1 h in 5% bovine serum albumin (BSA) or Milk in Tris-buffered saline containing 0.1% Tween-20 (TBST). Membranes were incubated with 5% BSA or Milk TBST primary antibody (NB 100-304, Novus Biologicals, Littleton Co; A5441 anti-β-actin, Sigma Aldrich, St. Louis, Mo; ab61783 p-KU70, AbCam, Cambridge, UK) overnight with shaking. Membranes were incubated for 1 h with goat anti-mouse-HRP or goat anti-rabbit-HRP (Cell Signalling, Billerica, Ma) in 5% BSA or Milk TBS-T. Blots were washed in TBS-T and incubated with Clarity™ Western ECL substrate (Bio Rad, Hercules, Ca) for 5 minutes before developing. Densitometry measurements were captured using the ChemiDoc station and software (Bio Rad, Hercules, Ca). All densitometric measurements were normalized to loading controls.

Cell cycle analysis

Cells were harvested by trypsinization, washed in PBS, and fixed overnight in 70% ethanol at 4 °C. Ethanol was removed by centrifugation and cells were washed with PBS, then resuspended and incubated 30 min at room temperature in Guava Cell Cycle Reagent containing propidium iodide. Cells were analyzed for DNA content on a Guava EasyCyte Mini flow cytometer using the Guava Cell Cycle program (Guava Technologies, Hayward CA).

SUPPLEMENTAL TAB.1 Cell culture strains and lines				
STRAIN NAME	SPECIES	COMMON NAME (strain)	ORIGIN (Age)	EXPERIMENTS
MEF	Mus musculus	Mouse	Embryo	FOCI, MN,
M3M	Mus musculus	Mouse	Adult (3 months)	FOCI, MN, WB, MTT
M2W	Mus musculus	Mouse	Young (2 weeks)	FOCI, MN, WB, MTT
3T3	Mus musculus	Mouse	Embryo (Immortalized)	FOCI, MN, COMET
YA35CF	Homo sapiens	Human	Adult (25 years)	FOCI, MN, WB, MTT
IMR90	Homo sapiens	Human	Embryo	FOCI, MN, COMET, WB
WI38	Homo sapiens	Human	Embryo	FOCI, MN
B#1	Bos taurus	Cow	Young (about 6 months)	FOCI, MN, COMET, MTT
D#1	Canis familiaris	Dog (Beagle)	Young – Adult	FOCI, MN, COMET, MTT
D#BAS	Canis familiaris	Dog (Basset hound)	Young – Adult	WB, MTT
LBB#4B	Myotis lucifugus	Little Brown Bat	Young – Adult (immortalized)	FOCI, MN, COMET, MTT

Supplementary Figure 1. Cell cycle progression after DNA damage was monitored by measuring DNA content on a Guava EasyCyte Mini flow cytometer. All cells were synchronized in G₀ phase by 48 h of serum starvation, and stimulated to enter into the S-phase by adding fresh regular growth medium. Cells in S-phase were treated with LD-ETO for 6 h in serum free medium. Cells were harvested by trypsinization and fixed overnight in 70%

ethanol at 4 °C. Fixed cells were prepared for cell cycle analysis by addition of Guava Cell Cycle Reagent containing propidium iodide.

Supplementary Figure 2. Immunoblot analysis for NEK4 and CYCLIN A in lysates from untreated (CTRL) or treated with LD-ETO for 6 hours, harvested at 24, 48 and 72 h after genotoxic treatment. Membranes were exposed for different intervals to obtain optimal signals. Actin and ponceau staining (protein) were used as loading controls.

Supplementary Figure 3. Mouse and Human cell populations were analyzed for the percentage of cells synthesizing DNA (BrdU positive throughout the nucleus; BrdU/TOT) and the percentage of cells that harbor BrdU-positive 53BP1 foci (% Nuclei with BrdU Foci) at 14, 24, and 72 h after LD-ETO treatment. For the 14 and 24 h time-points, the cultures were pulsed with BrdU for a 3 h period that began 10 h from the treatment period; the 72 h time-point was pulsed for 3 h beginning 24 h from the treatment period.

Supplementary Figure 4. ETO induces 53BP1 activation. A) Immunoblot analysis for 53BP1 in lysates from untreated control cultures (CTRL) or treated with LD-ETO (+) for 6 h, harvested at 6 or 24 h after genotoxic treatment. Membranes were exposed for different intervals to obtain optimal signals. Actin and Ponceau staining (protein) were used as loading controls. B) Quantification of 53BP1 signal, normalized over actin signal, is representative of two or more independent experiments. Statistical analysis: T-Student test followed by paired test (two tailed). The data from a single species were compared to each individual species for the same treatment time, and, inside a single species, CTRL values were compared with 6 and 24 h time points. Significant difference (p value <0,05) between pairs of species is indicated by the presence of a squared bracket or by the initials of each species (M = mouse; D = dog; C = cow; B = bat; H = human).

Fig. 1

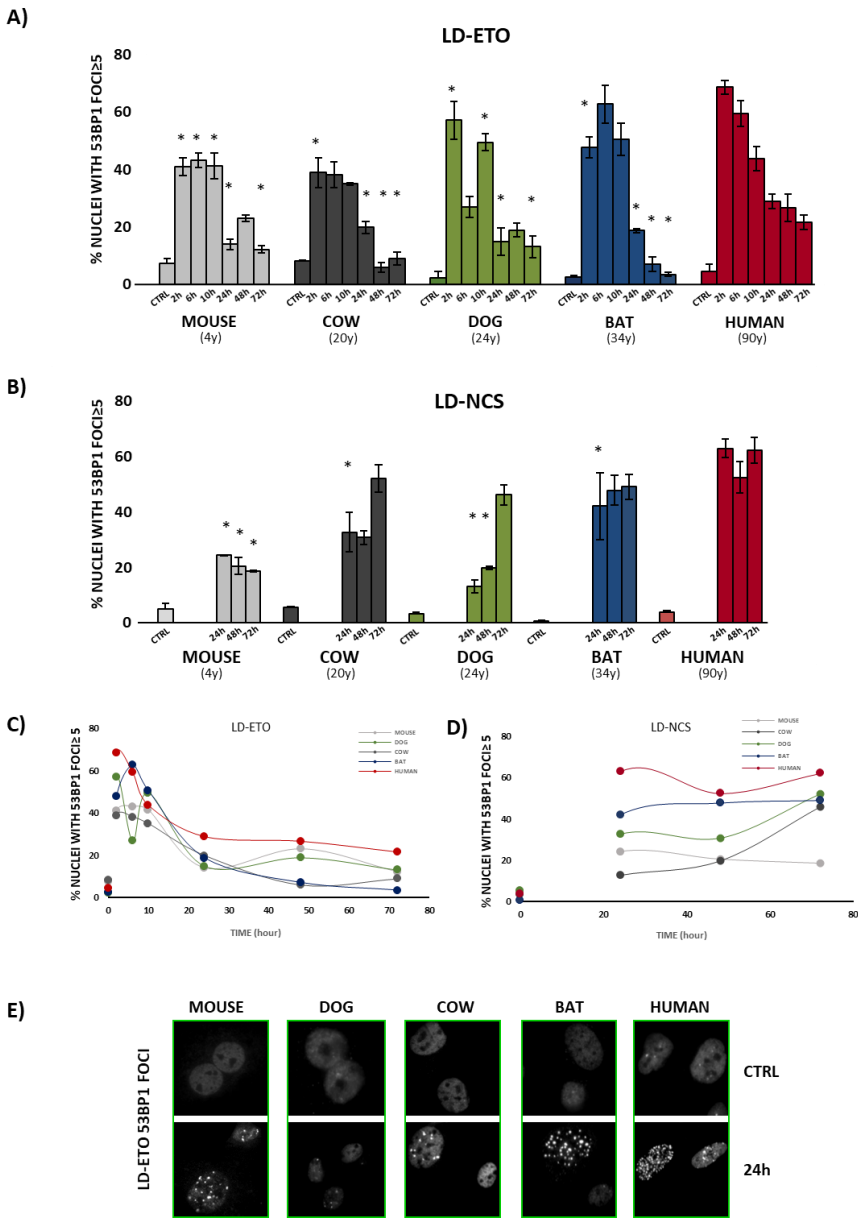


Fig. 2

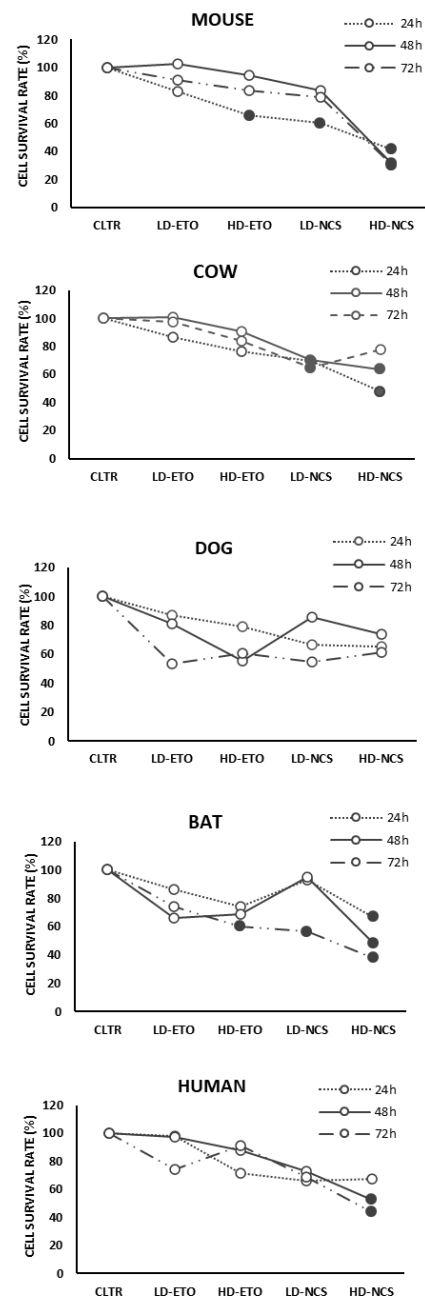


Fig. 3

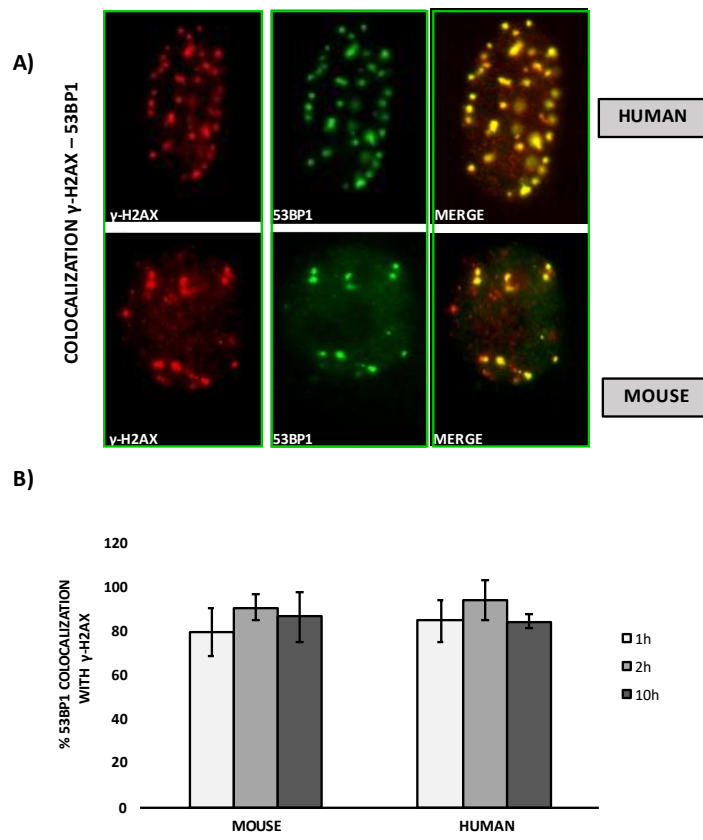


Fig. 4

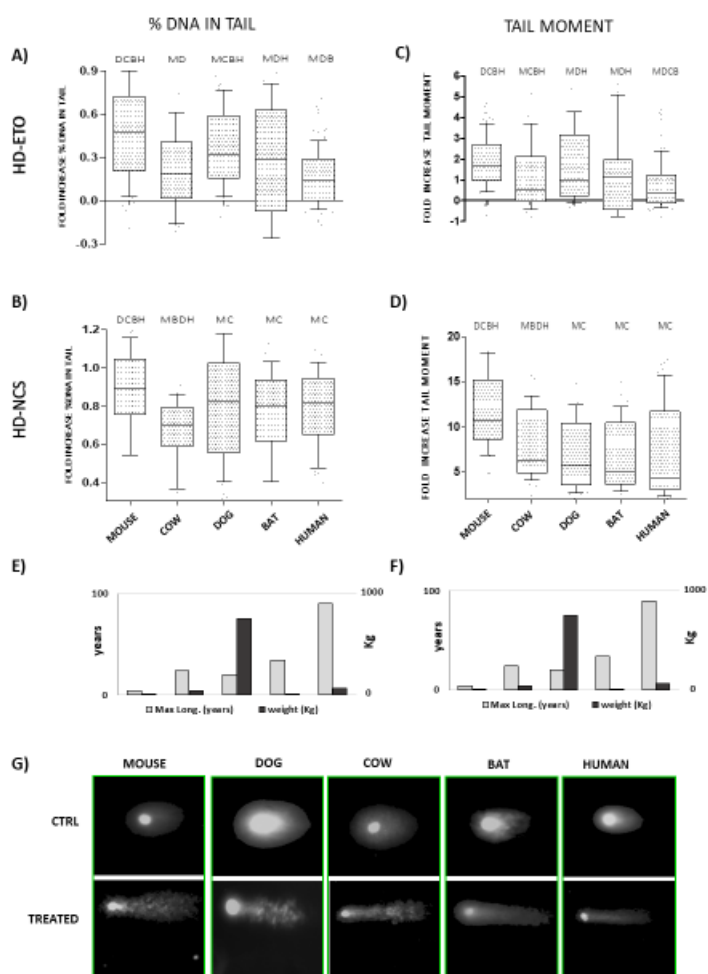


Fig. 5

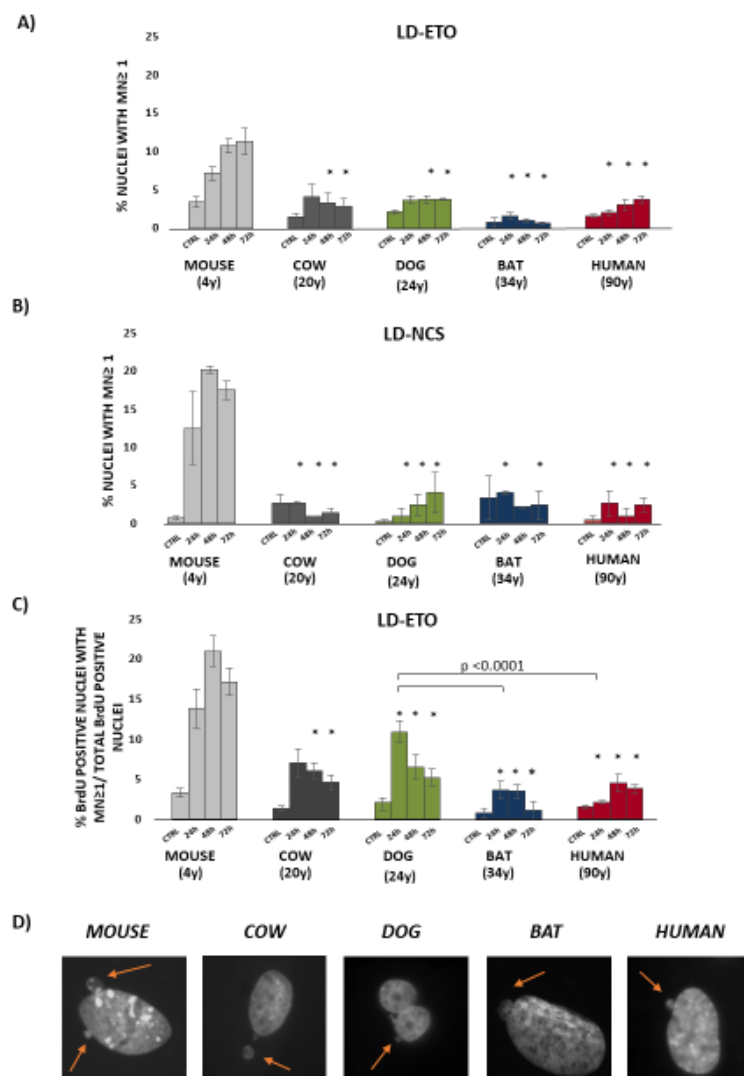


Fig. 6

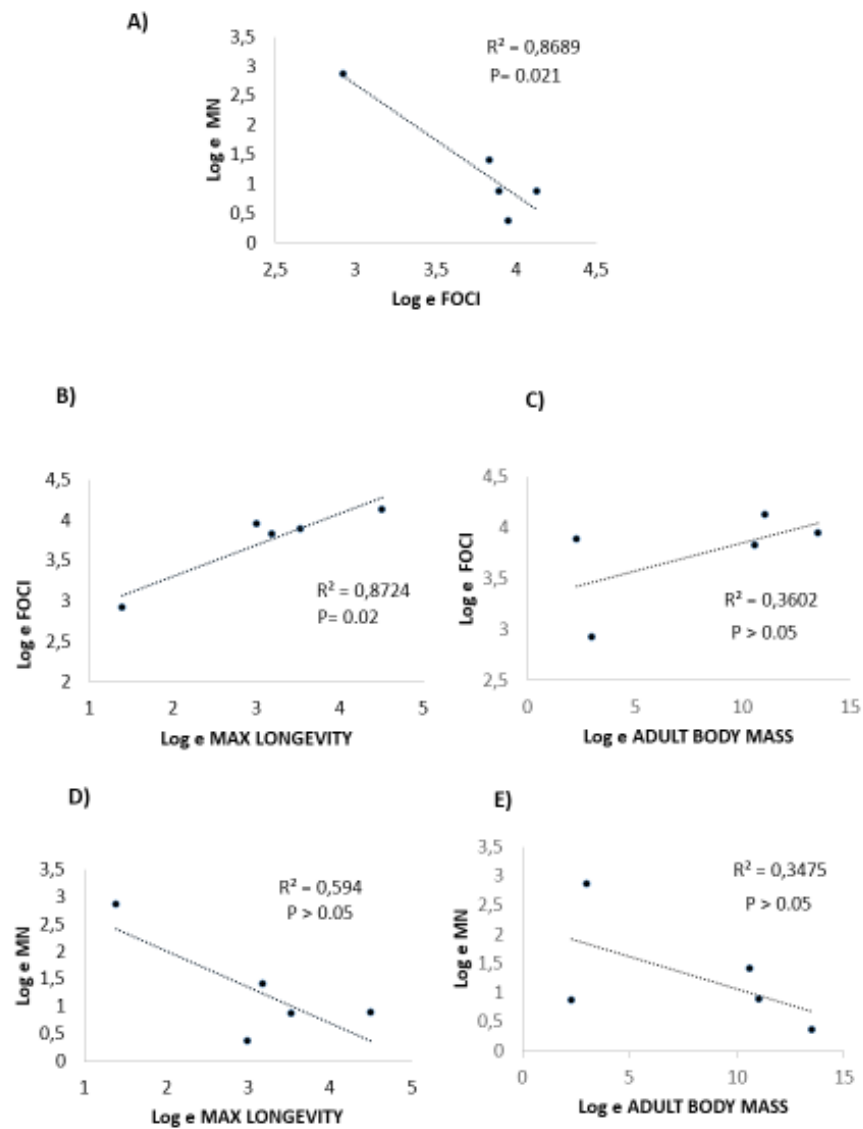
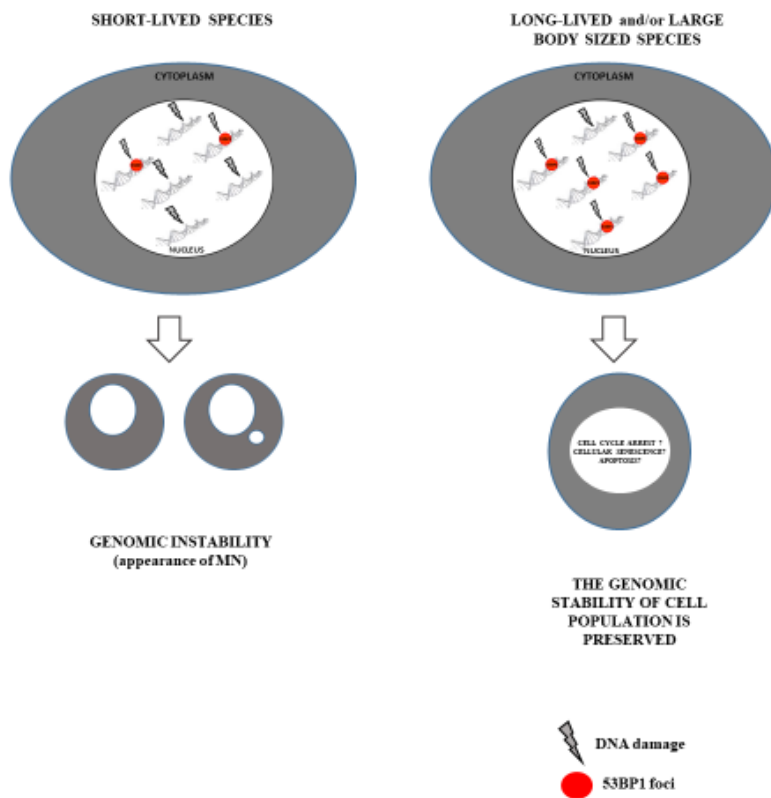
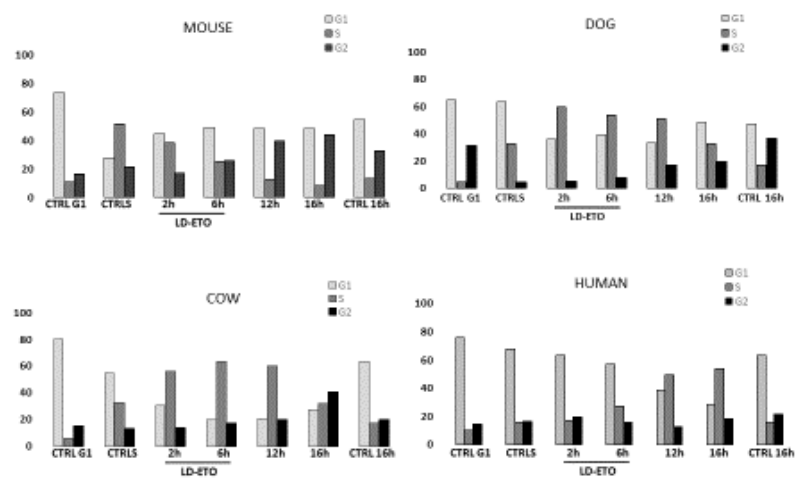


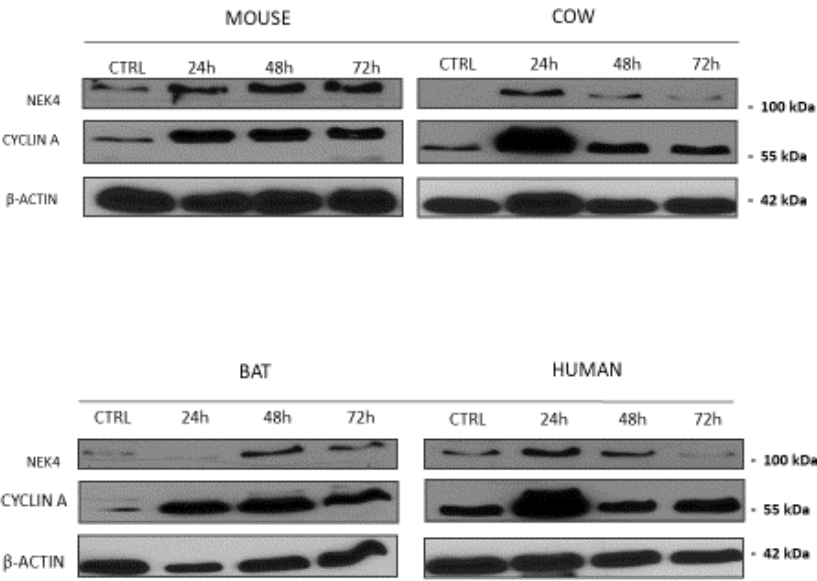
Fig. 7



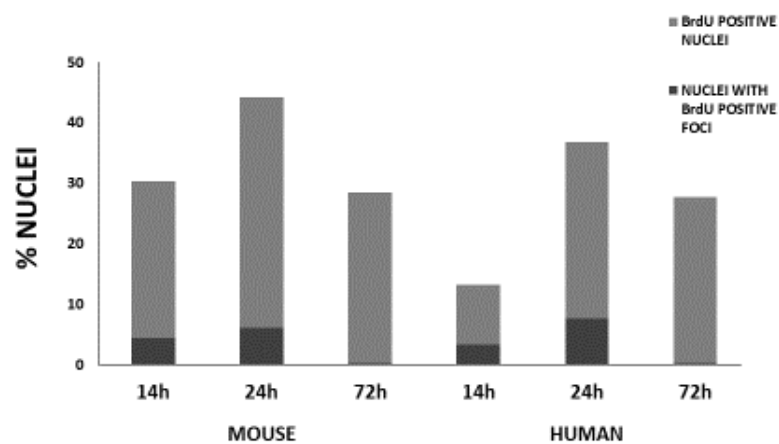
Supplementary Figure 1.



Supplementary Figure 2.

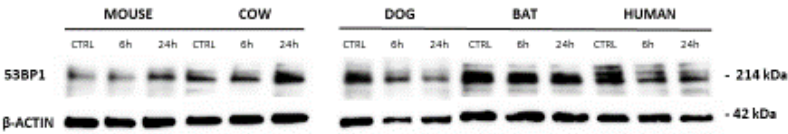


Supplemental Fig. 3



Supplementary Figure 4.

A)



B)

